

Calibrated Adversarial Sampling: Multi-Armed Bandit-Guided Generalization Against Unforeseen Attacks

Rui Wang¹ Zeming Wei¹

¹Peking University

Xiyue Zhang² Meng Sun¹

²University of Bristol

Abstract

Deep Neural Networks (DNNs) are known to be vulnerable to various adversarial perturbations. To address the safety concerns arising from these vulnerabilities, adversarial training (AT) has emerged as one of the most effective paradigms for enhancing the robustness of DNNs. However, existing AT frameworks primarily focus on a single or a limited set of attack types, leaving DNNs still exposed to attack types that may be encountered in practice but not addressed during training. In this paper, we propose an efficient fine-tuning method called *Calibrated Adversarial Sampling* (CAS) to address these issues. From the optimization perspective within the multi-armed bandit framework, it dynamically designs rewards and balances exploration and exploitation by considering the dynamic and interdependent characteristics of multiple robustness dimensions. Experiments on benchmark datasets show that CAS achieves superior overall robustness while maintaining high clean accuracy, providing a new paradigm for robust generalization of DNNs.

1. Introduction

Adversarial attacks [34] have posed significant vulnerabilities of Deep Neural Networks (DNNs), where adversaries can add imperceptible [6, 9] or semantic [11, 12] perturbations to craft adversarial examples that lead the target DNN to make incorrect predictions. So far, the existence of adversarial examples has raised serious concerns about the reliability of DNNs [17, 20, 21], compromising their safe and trustworthy deployment in real-world scenarios.

To address these concerns, numerous defense techniques in different DNN deployment stages have been proposed, such as adversarial training (AT) [24, 41, 45], robustness repair [5, 22, 33], and adversarial noise purification [4, 27, 44]. So far, most existing defenses only focus on a single robustness metric. However, in practice, DNN robustness encompasses multiple dimensions, with diverse metrics reflecting different types of vulnerabilities. Generally, adver-

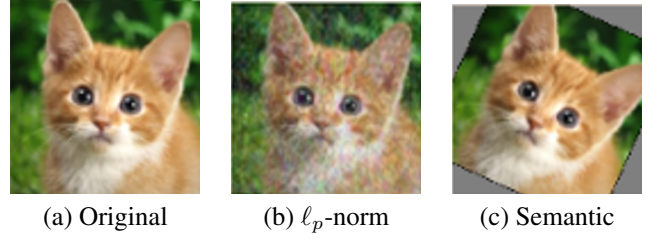


Figure 1. Illustration of adversarial perturbations by different attack types from [12].

sarial perturbations can be categorized into (i) **ℓ_p -norm perturbations**, and (ii) **semantic perturbations**.

For the ℓ_p -norm perturbation, a ℓ_p ball-constrained noise δ is added to the original input that $\|\delta\|_p \leq \epsilon$, where $p \in \{2, \infty\}$ is most commonly used. These perturbations are more imperceptible due to the ℓ_p -norm constraint, yet are difficult to reproduce or apply in real-world vision systems. Presently, existing AT research primarily focuses on this kind of ℓ_p -norm robustness of DNNs, with various techniques designed for a specific worst-case norm (typically ℓ_∞ or ℓ_2) [8, 24, 32, 39]. By contrast, semantic perturbation is crafted by applying realistic transformations to original inputs, *e.g.*, weather effects [13] or spatial transformations [43]. For instance, a DNN model in autonomous driving that fails to handle weather-induced corruptions (fog, snow) or geometric distortions (blur, rotation) could lead to catastrophic consequences. Examples of both types of perturbations are illustrated in Figure 1.

In this paper, we explore a new robust generalization paradigm through **fine-tuning pre-trained robust DNNs against unforeseen attacks**, *i.e.*, adversarial perturbations not encountered during the initial training phase. The motivation behind this paradigm is twofold. First, in practical deployment of DNNs, adversarially trained models remain vulnerable to previously unforeseen or unfocused attacks, while retraining the model from scratch to address these new threats is prohibitively expensive. Although previous AT methods explored generalizing under multiple robustness metrics, they require training models from scratch [25]. Thus, fine-tuning robust DNNs for generalizing against un-

foreseen attacks provides a feasible way to both leverage existing robustness and achieve new robust metrics. Furthermore, while a few preliminary frameworks explored fine-tuning DNNs for better robustness, they are limited to a fixed attack type (e.g., ℓ_p -norm attacks only) [7]. However, in safety-critical applications, models must endure multiple adversarial conditions simultaneously, including newly identified or considered semantic perturbations. Thus, we explore fine-tuning robust DNNs against unforeseen attacks to address these issues.

However, achieving this goal is hindered by several technical challenges. First, conventional multi-task learning approaches [3] incur computational costs that grow linearly with the number of adversarial attacks considered, making them impractical for real-world applications. On the other hand, probabilistic sampling-based methods that randomly select attack types face a complex variant of the multi-armed bandit problem [15], where the trade-off among different robustness types is intricate and challenging to balance during fine-tuning [38]. Such interaction between different adversarial perturbations can even degrade the overall multi-type robustness [13]. These issues highlight the need for a principled study of multi-dimensional robustness trade-offs, as well as a design of a specialized fine-tuning method tailored to their interactions.

To this end, we propose Calibrated Adversarial Sampling (CAS), a robust fine-tuning framework designed to balance the trade-offs among different robust metrics whilst generalizing against unforeseen attacks. Specifically, CAS employs a dynamic reward mechanism that holistically optimizes training resource allocation across attack types by accounting for cross-type trade-offs. Inspired by the Upper Confidence Bound (UCB) algorithm from multi-armed bandit theory, CAS further balances exploration and exploitation during the fine-tuning process (Figure 2). Extensive experiments on popular benchmark datasets from Robust-Bench [18] validate the effectiveness of CAS.

Our main contributions are summarized as follows:

- We formulate the multi-robustness fine-tuning problem within a multi-armed bandit framework, where adversarial sampling probabilities are dynamically adjusted to balance exploration and exploitation.
- We investigate the trade-offs among multiple robustness dimensions through both theoretical analysis and empirical studies. To the best of our knowledge, this is the first work to incorporate cross-type robustness trade-offs into fine-tuning strategies.
- We demonstrate that CAS achieves superior effectiveness and efficiency across benchmark datasets, providing a practical pathway toward robust DNN deployment in real-world applications.

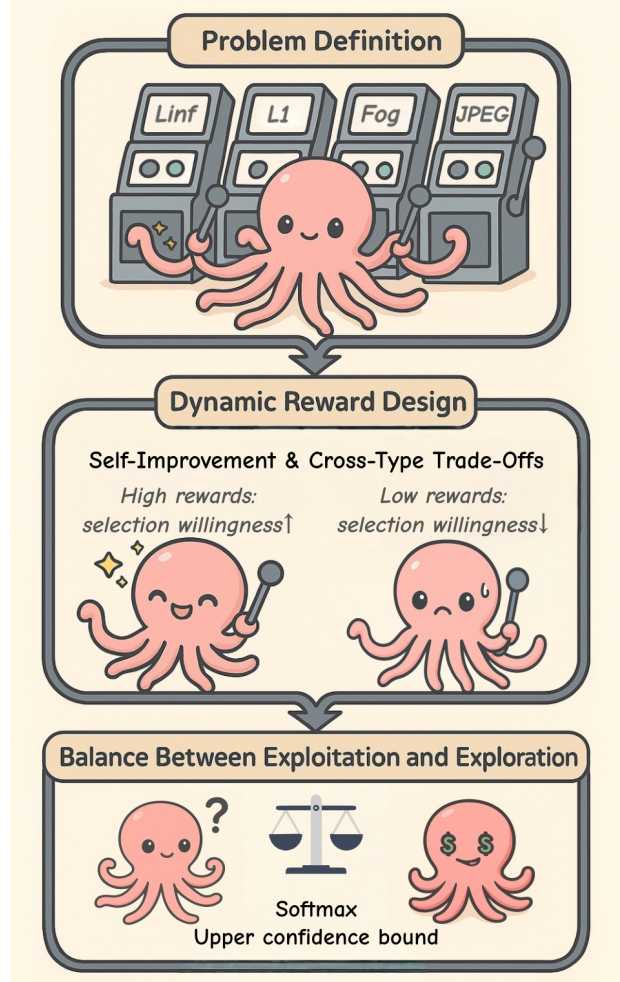


Figure 2. An overview of our CAS framework.

2. Related Work

2.1. Adversarial Examples

Adversarial examples are firstly discovered as deceptive samples crafted by applying subtle (often imperceptible) perturbations to clean inputs [34], which can mislead DNNs into making erroneous predictions. In practice, such perturbations are typically constrained within specific norm balls (e.g., ℓ_p -norm constraints). To deal with this threat, *adversarial training* (AT) has emerged as the primary defense paradigm [2, 32, 42], which enhances model robustness by explicitly injecting adversarial examples during training.

Notably, beyond ℓ_p -bounded “pixel-level” perturbations, there exists a challenging class of *semantic adversarial examples*. These adversarial examples leverage natural, semantically meaningful transformations (e.g., rotation, saturation, fog) to deceive models. They have different formal constraints and perturbation ranges, and are often more common in natural scenarios than pure ℓ_p attacks [12].

2.2. Multi-Robustness of DNNs

Although adversarial training with a single attack type can effectively improve robustness against that specific type of attack, real-world scenarios often require maintaining robustness against multiple kinds of potential adversarial perturbations. For example, a DNN used for medical image analysis may encounter deformations, flow-like distortions, and bubble artifacts. For ethical and safety considerations, it is essential to ensure that the used DNN model maintains a certain level of robustness against all these perturbations. Due to the large variety of attacks and the inherent trade-offs between different types of robustness [13], models trained from scratch often struggle to achieve both comprehensive robustness and fairness across attacks. In practice, fine-tuning is commonly used to efficiently obtain models that meet multiple robustness requirements. Stochastic adversarial training (SAT) [23] addresses this by randomly selecting attack types with fixed probabilities. E-AT [7] improves upon this by dynamically adjusting the selection probabilities based on robust accuracy, focusing more on relatively weaker robustness types. The AVG algorithm [36] adopts a multi-task training perspective by taking a weighted average of losses across different attacks, but when the number of attack types becomes large, this approach incurs significant computational overhead.

2.3. Multi-Armed Bandit Problem

The multi-armed bandit (MAB) problem is a classical framework for sequential decision-making under uncertainty, where an agent repeatedly selects from a set of actions (“arms”) and receives stochastic rewards [30]. The core challenge is to balance *exploration* (gathering information about uncertain arms) and *exploitation* (selecting arms believed to yield the highest rewards) [16]. Among the most widely used strategies for achieving this balance are the Upper Confidence Bound (UCB) algorithm [1] and Thompson Sampling [31, 35]. UCB methods construct optimistic confidence intervals around each arm’s estimated reward and select the arm with the highest upper bound. A detailed introduction and theoretical derivation of these two methods can be found in Appendix A.

3. Preliminaries

3.1. Unforeseen Adversarial Attacks

While significant breakthroughs have currently been achieved in research on ℓ_p robustness, such as AutoAttack [6], systematic investigations into semantic adversarial attacks remain comparably under-explored [6, 21]. Moreover, current robustness evaluations are often confined to single attack types, lacking a holistic framework that jointly considers diverse threat models. This narrow focus poses significant limitations for real-world AI deployments (*e.g.*,

autonomous driving, image processing systems), where robustness against physically plausible and naturalistic corruptions is critical for safety-critical applications [11, 40].

To enhance the versatility and comprehensiveness of robust fine-tuning methods in real-world applications, this work investigates *multi-robustness* under a broad and diverse set of adversarial attacks. From the framework proposed by [13], we select 17 representative semantic attacks for evaluation, including *Wood*, *Elastic*, *Pixel*, *Snow*, *Gabor*, *JPEG*, *Glitch*, *Kaleidoscope*, *Blur*, *Edge*, *Fog*, *Texture*, *Prison*, *Whirlpool*, *Polkadot*, *Klotski*, and *Hsv*. These cover a wide range of both environmental and digital perturbations that commonly arise in real-world settings. In addition, we incorporate the PerceptivePGD (PPGD) attack [46], a human-perception-guided method that explicitly models semantically meaningful visual changes, along with three standard ℓ_p -norm attacks: ℓ_∞ , ℓ_2 , and ℓ_1 . Together, this suite comprises 21 distinct adversarial attacks, enabling a comprehensive evaluation of model robustness against both semantic and norm-constrained perturbations.

3.2. Quantifying Mutually Exclusive Perturbations

Since our research comprehensively considers 21 adversarial attacks to transcend the limitations of AT against single adversarial attack, integrating diverse adversarial attacks into a unified AT framework introduces significant challenges. In particular, the Mutually Exclusive Perturbations (MEPs) [13] theory represents a fundamental limitation. MEPs occur when the constraint sets of two perturbation types are inherently incompatible, such that improving robustness against one attack inevitably degrades robustness against the other under fixed optimization conditions. Classic examples of this contradiction include the ℓ_p attack and the rotation-translation transformation as discussed in [13].

While the concept of MEPs qualitatively captures the inherent conflicts in achieving multi-robustness, it currently lacks a quantitative definition. To systematically quantify these phenomena, we conduct an empirical study based on the pre-trained ℓ_∞ -robust model [7] on the CIFAR-10 dataset [14], since ℓ_∞ pre-trained model exhibits inherent robustness against many adversarial attacks compared to a non-robust pre-trained model. In this experiment, we choose 11 perturbation types: ℓ_∞ , ℓ_2 , ℓ_1 , and 8 semantic attacks. For each attack type, we sequentially perform individual adversarial fine-tuning for 3 epochs and measure the robust accuracy against all 11 attacks before/after this fine-tuning. As illustrated in Figure 3, we observe several notable patterns. A more detailed analysis of this preliminary experiment can be found in Appendix E.

Semantic- ℓ_p Conflicts. As shown in Figure 3, semantic attacks often degrade ℓ_p robustness because most natural corruptions are incompatible with ℓ_p perturbation constraints.

Transfer Asymmetry. The tradeoff matrix shows no sym-

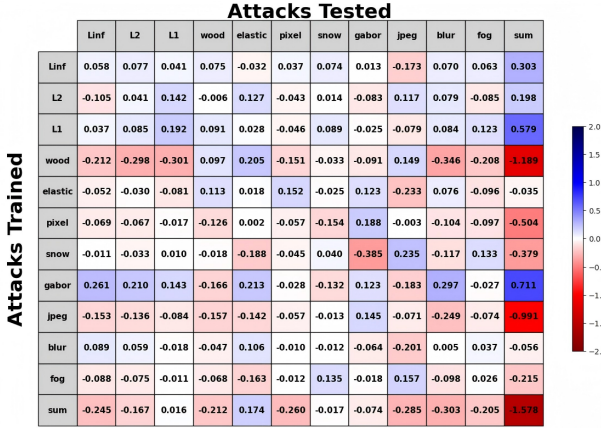


Figure 3. Trade-off matrix visualization. Each entry represents the change in robust accuracy of a specific attack type (shown along the top) after 3 epochs of sequential fine-tuning against designated attack types (shown on the left).

metric pattern with respect to the diagonal. For instance, ℓ_p adversarial training enhances robustness against most semantic attacks, while adversarial training using most semantic attacks tends to impair ℓ_p robustness.

Robustness Interference. When summing all values in the tradeoff matrix, it yields a notably negative total of **-1.578**. After fine-tuning with individual adversarial attacks, the overall robustness significantly decreases, indicating that the trade-off between multiple robustness presents a unique and challenging issue for our task.

3.3. Computational Analysis of Sequential Fine-Tuning Failure

The results of the preliminary experiment, where the sum of robust accuracies decreased after fine-tuning against individual adversarial attacks, have already demonstrated that such a simple sequential strategy is infeasible for multi-robustness fine-tuning. It is therefore necessary to adopt alternative strategies to mitigate these *cross-type trade-offs* and prevent *catastrophic forgetting* of previously trained attacks during fine-tuning. Before that, however, we first explore the theoretical reasons behind the failure of sequential fine-tuning to better understand this trade-off.

3.3.1. Theoretical Formulation

Let \mathcal{S}_p and \mathcal{S}_q denote two distinct attack types, each characterized by its perturbation range Δ_i for $i \in \{p, q\}$. The robust risk for each attack type $i \in \{p, q\}$ is defined as:

$$\mathcal{R}_i(\theta) = \mathbb{E}_{(x,y) \sim \mathcal{D}} \left[\max_{\delta \in \Delta_i} \mathcal{L}(f_\theta(x + \delta), y) \right], \quad (1)$$

where \mathcal{L} is the loss function, and \mathcal{D} denotes the clean data distribution. We then define the average robust risk as:

$$\mathcal{R}_{avg}(\theta) = \frac{1}{2}(\mathcal{R}_p(\theta) + \mathcal{R}_q(\theta)). \quad (2)$$

3.3.2. Main Results

Lemma 1 (Average robust risk bound) *The change in average robust risk $\Delta\mathcal{R}_{avg}$ can be bounded as:*

$$\Delta\mathcal{R}_{avg} \lesssim -\|\nabla\mathcal{R}_{avg}(\theta_1)\| \|\Delta\theta\| \cos \psi + \frac{1}{2} \lambda_{\max}(H_{avg}) \|\Delta\theta\|^2 \quad (3)$$

where ψ denotes the angle between $\nabla\mathcal{R}_{avg}(\theta_1)$ and $\nabla\mathcal{R}_q(\theta_1)$, H_{avg} is the local Hessian of \mathcal{R}_{avg} , $\lambda_{\max}(H_{avg})$ denotes its largest eigenvalue of the Hessian at θ_1 .

Based on the preceding lemma, we can derive a safe parameter-drift threshold to prevent the average robust risk from increasing during fine-tuning

Proposition 1 (Safe parameter-drift threshold) *Let*

$\lambda_{\max}(H_{avg})$ denote the largest eigenvalue of the local Hessian of \mathcal{R}_{avg} at θ_1 . A sufficient condition to prevent average robustness degradation after the sequential fine-tuning in the order of S_p followed by S_q is:

$$\|\Delta\theta\| < \frac{2\|\nabla\mathcal{R}_{avg}(\theta_1)\| \cos \psi}{\lambda_{\max}(H_{avg})}, \quad \psi < \frac{\pi}{2} \quad (4)$$

This reveals that degradation arises either from strong gradient alignment (ψ is relatively large), excessive drift $\Delta\theta$, or from large curvature $\lambda_{\max}(H_{avg})$. The detailed assumptions and proofs are provided in Appendix B.

3.3.3. Empirical Understanding

Based on Proposition 1, we identify *parameter drift* as the primary mechanism behind the failure of sequential fine-tuning. A sufficiently large displacement in parameter space can push the model out of regions robust to previous attack types, leading to *catastrophic forgetting*. This parameter drift arises mainly from *gradient conflicts* among different adversarial objectives, which fundamentally stem from distinct constraint structures of these attacks. Moreover, excessive optimization on a single adversarial distribution further amplifies such drift, exacerbating catastrophic forgetting. Empirically, we find that baseline strategies, such as random sampling or joint optimization over multiple attack losses, effectively mitigate parameter drift and thus reduce the trade-off among different robustness objectives. In contrast, sequential fine-tuning inherently amplifies this drift beyond the stability threshold.

These observations motivate the design of our Calibrated Adversarial Sampling (CAS) method. CAS employs high-frequency random sampling to counteract parameter drift and explicitly incorporates the cross-type trade-off among multiple robustness objectives. This enables it to optimize parameter updates along safer directions and maintain balanced robustness across attacks. Furthermore, inspired by multi-objective optimization theory, we introduce the cross-type trade-off structure into the reward function to guide updates along the *Pareto frontier*, balancing exploration and exploitation, as detailed in Appendix C.

4. Methodology

We cast the problem of fine-tuning for multi-type robustness as a complex variant of the multi-armed bandit problem. By designing a dynamic and fair reward function and balancing exploration with exploitation, we transform the complex problem of jointly optimizing multiple robustness objectives into an interpretable and extensible framework, named Calibrated Adversarial Sampling (CAS), as illustrated in Figure 2.

4.1. Problem Formulation

Consider a classification model f_θ trained on data distribution \mathcal{D} , and a set of M adversarial perturbation types $\mathcal{P} = \{p_1, p_2, \dots, p_M\}$. Each p_k corresponds to an adversarial attack type (e.g., ℓ_∞ , blur) and has an importance weight w_k . At each training iteration t , we select a perturbation type p_{a_t} , generate adversarial examples under this type, and update model parameters $\theta_t \mapsto \theta_{t+1}$ accordingly.

We view the choice of p_{a_t} as pulling arm a_t in a multi-armed bandit. The “reward” quantifies the overall improvement in multi-type robustness achieved by training on this perturbation type. However, unlike standard bandits, the underlying reward process here is:

- **Non-stationary:** The robustness improvement achieved by each adversarial training step is not fixed, and can only be dynamically evaluated through the loss and robust accuracy on the corresponding adversarial examples.
- **Partially observable:** Adversarial training against one perturbation can simultaneously increase or decrease robustness against other perturbations. Since the real-time impact against other perturbation types cannot be directly observed, these dynamics are thus better modeled as a partially observable Markov process.

Formally, let $L_m^{(t)}$ denote the adversarial loss under perturbation p_m at iteration t , with the observed feedback given by the loss sequence $(L_{k_0}^{(0)}, L_{k_1}^{(1)}, \dots, L_{k_t}^{(t)})$. Since the evolution of multi-type robustness is unknown and potentially non-stationary, designing a comprehensive and dynamic reward function is challenging yet crucial.

4.2. Reward Design

At each iteration, the reward for selecting perturbation p_v is composed of two parts:

$$R_v = R_v^{\text{self}} + R_v^{\text{tradeoff}} \quad (5)$$

where R_v^{self} captures the marginal gain in robustness under p_v itself, and R_v^{tradeoff} measures its effect on other perturbation types.

Marginal Robustness Gain. To reliably estimate the marginal effect of training against p_v attack, we examine

the trajectory of $\log L_v^{(t)}$ over a sliding window that records the most recent W iterations:

$$R_v^{\text{self}} = -\text{slope}(\log L_v^{(t-W+1)}, \dots, \log L_v^{(t)}) \cdot w_v. \quad (6)$$

Here, $\text{slope}(\cdot)$ denotes the slope of the linear regression line fitted to the pairs $(i, \log L_v^{(i)})$, where $i = t - W + 1, \dots, t$. Applying the logarithm promotes fairness across different adversarial training types by normalizing loss magnitudes, which can vary significantly between attacks, and reducing sensitivity to the perturbation strength ϵ_k . The sliding window smooths noises while capturing recent trends, and a steeper negative slope indicates faster robustness improvement.

Cross-Type Trade-off. Training on p_v may affect losses under other perturbations p_k ($k \neq v$), occasionally yielding improvements but often causing degradation due to conflicting constraints (Figure 3). To quantify this, we maintain for each p_k a dynamic record of which other perturbations were trained between its two most recent updates, along with their counts. If perturbation p_v was selected $n_{v,k}$ times in this interval, its trade-off contribution to p_k is weighted proportionally. Summing over all affected p_k gives

$$R_v^{\text{tradeoff}} = \sum_{k \neq v} w_k \cdot \frac{n_{v,k}}{\sum_{j=1}^M n_{j,k}} \cdot \log \frac{L_k^{(t_{\text{prev}})}}{L_k^{(t_{\text{curr}})}} \quad (7)$$

where t_{curr} and t_{prev} are the two most recent occurrences of p_k . This term rewards perturbation types that induce favorable cross-type transfer and penalizes those causing degradation. Using logarithmic loss differences ensures scale-invariance and enhances fairness across perturbations.

Hybrid Loss. To balance clean accuracy and robustness, we adopt a TRADES-style [45] hybrid loss:

$$\mathcal{L}_{\text{total}} = \beta \mathcal{L}(f_\theta(x^{\text{adv}}), y) + (1 - \beta) \mathcal{L}(f_\theta(x), y) \quad (8)$$

where x^{adv} is the adversarial example generated under the selected perturbation type, and β is a weighting hyperparameter. This formulation prevents catastrophic degradation of clean accuracy during adversarial training.

4.3. Balancing Exploration and Exploitation

To effectively fine-tune across multiple perturbation types, it is essential to balance *exploitation*, focusing on high-reward perturbations with *exploration* of under-sampled ones to ensure accurate update of rewards for all perturbation types. To achieve this, we utilize the Upper Confidence Bound (UCB) algorithm from multi-armed bandit theory in our sampling strategy.

Let N_v denote the number of times perturbation p_v has been selected (initialized as $N_v = 1$). The final selection score is defined as:

$$\tilde{R}_v = \exp(\alpha \cdot R_v) + \sqrt{\frac{2 \log(\sum_{j=1}^M N_j)}{N_v}}, \quad (9)$$

where a is a hyperparameter that controls the scaling of rewards. The exponential term ensures non-negativity and enables smooth weighting under the softmax sampling scheme, while the second term encourages exploration by increasing the score for rarely-sampled perturbations. As training progresses and N increases, the exploration term gradually diminishes in magnitude relative to N_v , naturally shifting the selection strategy from exploration toward exploitation. Sampling probabilities are then defined as:

$$\pi_v = \frac{\tilde{R}_v \cdot w_v}{\sum_{j=1}^M \tilde{R}_j \cdot w_j}, \quad (10)$$

where w_v denotes an optional user-specified importance weight. At each iteration, perturbation types are chosen according to π_v . This strategy allows CAS to adaptively allocate adversarial samples towards those with higher overall robustness gains while ensuring sufficient exploration to maintain fairer coverage and mitigate catastrophic forgetting of previously trained types.

Algorithm 1 Calibrated Adversarial Sampling (CAS)

Require: Pre-trained model parameters θ , perturbations $\mathcal{P} = \{p_1, \dots, p_M\}$ with weights w_1, \dots, w_M , sliding window size W , hyperparameter α and β , total iterations T

Ensure: Fine-tuned model parameters θ_T

- 1: Initialize $N_v \leftarrow 0$ for all $v \in [M]$, loss history buffers
- 2: **for** $t = 1$ to T **do**
- 3: **for** $v = 1$ to M **do**
- 4: $R_v^{\text{self}} \leftarrow -\text{slope}(\log L_v^{(t-W+1)}, \dots, \log L_v^{(t)}) \cdot w_v$
- 5: Compute R_v^{tradeoff} using loss buffers and cross-type records (Eq. 7)
- 6: $R_v \leftarrow R_v^{\text{self}} + R_v^{\text{tradeoff}}$ {Compute reward}
- 7: $\tilde{R}_v \leftarrow \exp(\alpha \cdot R_v) + \sqrt{\frac{2 \log(\sum_{j=1}^M N_j)}{N_v}}$ {Softmax and UCB augmentation}
- 8: **end for**
- 9: Sample $a_t \sim \pi$ where $\pi_v = \frac{\tilde{R}_v \cdot w_v}{\sum_j \tilde{R}_j \cdot w_j}$
- 10: $N_{a_t} \leftarrow N_{a_t} + 1$
- 11: Generate x^{adv} under perturbation p_{a_t}
- 12: $\mathcal{L}_{\text{total}} \leftarrow \beta \mathcal{L}(f_{\theta}(x^{\text{adv}}), y) + (1 - \beta) \mathcal{L}(f_{\theta}(x), y)$
- 13: Update θ_t via $\nabla_{\theta} \mathcal{L}_{\text{total}}$
- 14: Update $L_{a_t}^t$ and cross-type records
- 15: **end for**

5. Experiment

In this section, we demonstrate the effectiveness of our proposed CAS framework in improving overall robustness and addressing the multi-robust trade-off.

5.1. Experimental Setup

We conduct our experiments on the benchmark datasets CIFAR-10, CIFAR-100 [14] and SVHN [26] using pre-trained PreActResNet-18 [10] models provided by [7] and [29]. During fine-tuning, we consider the 21 different adversarial attacks presented in Section 3.1.

Baselines. We compare our CAS method with two representative high-frequency random fine-tuning baselines: SAT [23] and E-AT [7]. To examine whether the order of adversarial attacks affects performance, we also include a simple sequential fine-tuning scheme of our own design, which cycles through attack types in a fixed, weight-based order. Additionally, we add the well-known AVG method [36] for the comparison of different random fine-tuning and multi-task learning methods. Detailed descriptions of SAT, E-AT, and AVG are provided in Section 2.

Training Settings. Following the common practice of AT [28, 37, 41], we fine-tune a pretrained PreActResNet-18 model using SGD with momentum 0.9, weight decay 5×10^{-4} , and initial learning rate 0.1 for 10 epochs. The hyperparameters are set to $\alpha = 10$ and $\beta = \frac{8}{9}$. On CIFAR-10 the pretrained model has been adversarially trained under the ℓ_{∞} norm, while on CIFAR-100 and SVHN, the models have been adversarially trained under ℓ_2 . We limit the number of fine-tuning epochs as prior work [7] has shown that quick fine-tuning can significantly improve multi-robustness, which is also corroborated by our own ablation study.

All ℓ_p attacks are conducted using default perturbation margin $\epsilon_{\infty} = \frac{8}{255}$, $\epsilon_2 = 0.5$, and $\epsilon_1 = 12$. For semantic attacks, we compute a calibrated margin iteratively to ensure that most perturbations yield robust accuracies between 20% and 60% on the pre-trained CIFAR-10 model:

$$\epsilon_k = (\lambda_k + acc_{\text{adv}}[k]) \times \epsilon \quad (11)$$

where ϵ is the original perturbation margin and λ_k is a hyperparameter controlling the calibration. We repeat this process until the robust accuracy $acc_{\text{adv}}[k]$ falls within the desired range.

Evaluation Metrics. We report the mean and standard deviation of both clean and robust accuracy over five independent runs. Robust accuracy is evaluated by AutoAttack [6], a widely-used robustness evaluation benchmark.

Real-World Scenario Simulation. On CIFAR-10 and CIFAR-100, we assign weight 6 to ℓ_{∞} , ℓ_2 , and ℓ_1 attacks, and weight 1 to the 18 semantic attacks. This setup emulates a scenario where attackers can precisely manipulate

Table 1. Overall comparison of our CAS method with baselines on CIFAR-10, CIFAR-100 and SVHN datasets. The “Original” model is obtained via ℓ_p pre-training on each dataset, and “Order” denotes sequential fine-tuning by cycling through attack types in a fixed order. **avg.** ℓ_p denotes the average robust accuracy over ℓ_∞ , ℓ_2 , and ℓ_1 , while **avg. Corruption** denotes the average robust accuracy against snow, fog, and blur attacks. All results are reported as mean \pm standard deviation over five independent runs.

Dataset	Accuracy	Original	E-AT	SAT	Order	AVG	CAS (ours)
CIFAR-10	Clean	82.90 \pm 0.00	83.56 \pm 0.31	84.62 \pm 0.42	82.92 \pm 0.17	84.56 \pm 0.24	85.26\pm0.33
	avg. Robust	33.51 \pm 0.00	51.50 \pm 0.33	51.41 \pm 0.40	51.23 \pm 0.15	51.46 \pm 0.23	51.79\pm0.35
	avg. ℓ_p	31.13 \pm 0.00	52.86 \pm 0.60	53.81 \pm 0.54	53.95\pm0.18	53.47 \pm 0.31	52.91 \pm 0.54
	avg. Semantic	35.88 \pm 0.00	50.14 \pm 0.31	49.00 \pm 0.27	48.51 \pm 0.13	49.46 \pm 0.18	50.67\pm0.22
CIFAR-100	Clean	48.00 \pm 0.00	57.40 \pm 0.39	57.92 \pm 0.50	56.94 \pm 0.31	57.78 \pm 0.30	58.54\pm0.48
	avg. Robust	16.61 \pm 0.00	27.62 \pm 0.48	27.53 \pm 0.46	27.12 \pm 0.30	27.43 \pm 0.32	27.99\pm0.37
	avg. ℓ_p	19.03 \pm 0.00	28.60 \pm 0.67	28.69 \pm 0.50	28.75 \pm 0.29	28.56 \pm 0.37	29.23\pm0.46
	avg. Semantic	14.19 \pm 0.00	26.65 \pm 0.43	26.36 \pm 0.46	25.48 \pm 0.33	26.29 \pm 0.32	26.75\pm0.39
SVHN	Clean	80.40 \pm 0.00	92.06 \pm 0.46	93.32 \pm 0.66	92.82 \pm 0.35	93.02 \pm 0.39	93.86\pm0.54
	avg. Robust	40.20 \pm 0.00	56.32 \pm 0.71	55.91 \pm 0.73	53.03 \pm 0.49	56.33 \pm 0.41	57.76\pm0.67
	avg. Corruption	41.67 \pm 0.00	62.86 \pm 0.67	63.62 \pm 0.52	60.63 \pm 0.66	63.51 \pm 0.44	63.81\pm0.48
	avg. Others	38.74 \pm 0.00	49.78 \pm 1.05	48.21 \pm 1.05	45.43 \pm 0.75	49.15 \pm 0.58	51.71\pm0.96

Table 2. Average fine-tuning time cost on three datasets.

	E-AT	SAT	Order	AVG	CAS
Time (s)	2390.7	2386.6	2375.4	47241.1	2408.0

inputs by adding small perturbations, motivating defenses focusing on norm-constrained attacks. For the street-view SVHN dataset, we assign weight 6 to common corruptions (snow, blur, and fog) and weight 1 to the remaining 18 attacks, simulating an autonomous driving context where robustness to natural corruptions is critical. The final average robust accuracy is the weighted sum of individual robust accuracy using these scenario-specific weights.

5.2. Main Results

Superior Holistic Accuracy. As shown in Table 1, our CAS method achieves the highest clean accuracy and the best average robust accuracy on all datasets. It consistently delivers strong performance on CIFAR-10, CIFAR-100, and SVHN, while maintaining balanced robustness between high-weighted and other perturbation types. Notably, on SVHN, CAS surpasses all baselines by at least 1.4% in average robust accuracy, demonstrating its potential for real-world scenarios such as autonomous driving. These improvements mainly stem from our reward design that explicitly accounts for robustness trade-offs, together with the UCB-based exploration-exploitation mechanism. The effectiveness of these components is further validated through ablation studies in Appendix F.

Analysis of Baselines. Each baseline exhibits distinct characteristics. E-AT adaptively assigns higher selection probability to attacks with lower robust accuracy, enhancing fair-

ness across robustness types; however, this tendency to favor stronger attacks often reduces clean accuracy. The random fine-tuning method SAT and the multi-task learning approach AVG yield similar performance, as analyzed from a Pareto frontier perspective in Appendix C. The “Order” method exhibits lower variance than random methods, but also lower accuracy, suggesting that a fixed order of attack selection may induce overfitting to the sampling sequence, thereby degrading overall performance.

Time Cost Analysis. As reported in Table 2, our CAS method improves final accuracy with a comparable time cost to other baseline methods while outperforming the AVG method. The time cost of AVG grows linearly with the number of adversarial attack types, revealing an inherent limitation of multi-task learning methods in scalability.

5.3. Ablation and Sensitivity Analysis

Epochs. The analysis results on training epochs (Figure 4) validate our choice of 10 epochs for the main experiments. During initial training (epochs 0-6), all methods exhibit significant instability in accuracy. This aligns with prior findings that, in the early stages of adversarial training, the loss surface has not yet been smoothed, and optimization conflicts occur while the model learns robust features [19, 45, 47]. Beyond epoch 10, clean accuracy stabilizes and robust accuracy shows only marginal fluctuations with diminishing returns. Our CAS method demonstrates stable superiority in this regime, maintaining robustness advantages without compromising clean performance. Therefore, 10 epochs represent an optimal trade-off between performance and efficiency, avoiding unnecessary computational and overfitting risk while achieving strong multi-robustness.

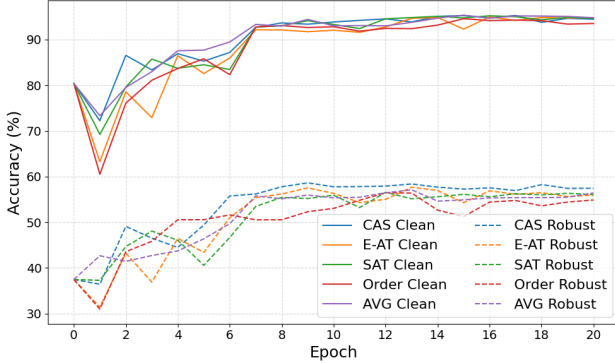


Figure 4. Ablation study examining the effect of training epochs using SVHN. Robust accuracy is the weighted average, and all results are reported as the mean over five independent runs.

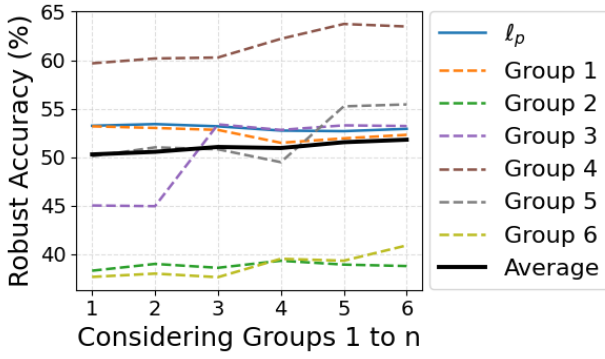


Figure 5. Ablation study on the number of considered perturbations using CIFAR-10. The 18 semantic attacks (Wood, Elastic, Pixel, Snow, Gabor, JPEG, Glitch, Kaleidoscope, Blur, Edge, Fog, Texture, Prison, Whirlpool, Polkadot, Klotski, and Hsv) are divided into six groups, each containing three attacks in order from left to right. These groups are gradually incorporated, along with the three ℓ_p attacks, into CAS fine-tuning. The ℓ_p attacks are assigned a weight of 6, and all considered semantic attacks are assigned with a weight of 1. We report the average robust accuracy within each group and the weighted average accuracy across all attacks. Results are averaged over five independent runs.

Number of Considered Perturbations. As shown in Figure 5, incorporating more perturbation types during fine-tuning steadily improves the overall average robust accuracy, while the ℓ_p robustness shows a slight but stable decline. The robustness trends of different semantic attack groups also vary: for instance, the robustness of Group 3 and Group 5 show clear improvement when they are included in fine-tuning, whereas Group 1 and Group 5 experience minor degradation when Group 4 is introduced, indicating a negative trade-off caused by that group. In contrast, Group 2 appears insensitive to the inclusion of other attacks. Overall, expanding the range of perturbation types

Table 3. Sensitivity analysis of the hyperparameter α , which controls the balance between exploration and exploitation in CAS, conducted on the CIFAR-10 dataset. Results are averaged over five independent runs.

α	1	5	10	20	50
Clean	84.32	84.68	85.26	85.42	85.04
avg. Robust	51.68	51.50	51.79	51.55	50.83
avg. ℓ_p	53.10	53.27	52.91	52.83	50.60
avg. Semantic	50.26	49.73	50.67	50.26	51.05

in CAS fine-tuning yields a stable improvement in average robustness, with only limited negative effects on specific robustness types. These observations suggest that, in practice, introducing a broader variety of adversarial attacks during fine-tuning enhances general robustness.

Bias between Exploration and Exploitation. According to Eq. 9, a larger α makes the CAS method more inclined toward exploitation, while a smaller α encourages exploration. As shown in Table 3, gradually increasing α from 1 to 10 improves both clean accuracy and robustness. This is because a moderate increase in α enables CAS to better utilize reward information for optimal sampling allocation, thereby mitigating negative trade-offs. However, since α affects the reward exponentially in Eq. 9, excessively large α values cause CAS to overemphasize high-reward adversarial perturbations, leading to degradation in multi-robustness and increasing the risk of catastrophic forgetting. Empirically, setting α between 10 and 20 achieves a good balance between exploration and exploitation.

Additional analysis. We provide more comprehensive ablation studies on more datasets and each key component in Appendix F, where the results are consistent with claims in this section.

6. Conclusion

In this paper, we introduced Calibrated Adversarial Sampling (CAS), a novel fine-tuning framework designed to enhance the multi-robustness of DNNs against a broad range of unforeseen adversarial attacks. Through theoretical analysis and empirical evaluation on mutually exclusive perturbations, we investigated the inherent cross-type trade-offs among multiple robustness dimensions and developed a dynamic reward mechanism to address them. Our framework bridges the multi-armed bandit framework and multi-robustness fine-tuning, enabling principled and efficient adversarial sampling. Extensive experiments demonstrate that CAS achieves superior robustness and computational efficiency across diverse attack scenarios, establishing a practical paradigm for real-world robust generalization of DNNs.

References

[1] Peter Auer. Using confidence bounds for exploitation-exploration trade-offs. *Journal of machine learning research*, 3(Nov):397–422, 2002. 3

[2] Tao Bai, Jinqi Luo, Jun Zhao, Bihan Wen, and Qian Wang. Recent advances in adversarial training for adversarial robustness. *arXiv preprint arXiv:2102.01356*, 2021. 2

[3] Rich Caruana. Multitask learning. *Machine learning*, 28(1): 41–75, 1997. 2

[4] Huanran Chen, Yinpeng Dong, Shitong Shao, Hao Zhongkai, Xiao Yang, Hang Su, and Jun Zhu. Diffusion models are certifiably robust classifiers. *Advances in Neural Information Processing Systems*, 37:50062–50097, 2024. 1

[5] Zhiming Chi, Jianan Ma, Pengfei Yang, Cheng-Chao Huang, Renjue Li, Xiaowei Huang, and Lijun Zhang. Patch synthesis for property repair of deep neural networks. *arXiv preprint arXiv:2404.01642*, 2024. 1

[6] Francesco Croce and Matthias Hein. Reliable evaluation of adversarial robustness with an ensemble of diverse parameter-free attacks. In *International conference on machine learning*, pages 2206–2216. PMLR, 2020. 1, 3, 6

[7] Francesco Croce and Matthias Hein. Adversarial robustness against multiple and single l_p -threat models via quick fine-tuning of robust classifiers. In *International Conference on Machine Learning*, pages 4436–4454. PMLR, 2022. 2, 3, 6

[8] Yinpeng Dong, Ke Xu, Xiao Yang, Tianyu Pang, Zhijie Deng, Hang Su, and Jun Zhu. Exploring memorization in adversarial training. *arXiv preprint arXiv:2106.01606*, 2021. 1

[9] Ian J Goodfellow, Jonathon Shlens, and Christian Szegedy. Explaining and harnessing adversarial examples. *arXiv preprint arXiv:1412.6572*, 2014. 1

[10] Kaiming He, Xiangyu Zhang, Shaoqing Ren, and Jian Sun. Identity mappings in deep residual networks. In *European conference on computer vision*, pages 630–645. Springer, 2016. 6

[11] Dan Hendrycks and Thomas Dietterich. Benchmarking neural network robustness to common corruptions and perturbations. *arXiv preprint arXiv:1903.12261*, 2019. 1, 3

[12] Lei Hsiung, Yun-Yun Tsai, Pin-Yu Chen, and Tsung-Yi Ho. Towards compositional adversarial robustness: Generalizing adversarial training to composite semantic perturbations. In *Proceedings of the IEEE/CVF conference on computer vision and pattern recognition*, pages 24658–24667, 2023. 1, 2

[13] Daniel Kang, Yi Sun, Dan Hendrycks, Tom Brown, and Jacob Steinhardt. Testing robustness against unforeseen adversaries. 2019. 1, 2, 3

[14] Alex Krizhevsky, Geoffrey Hinton, et al. Learning multiple layers of features from tiny images. 2009. 3, 6

[15] Volodymyr Kuleshov and Doina Precup. Algorithms for multi-armed bandit problems. *arXiv preprint arXiv:1402.6028*, 2014. 2

[16] Tor Lattimore and Csaba Szepesvári. *Bandit algorithms*. Cambridge University Press, 2020. 3

[17] Bo Li, Peng Qi, Bo Liu, Shuai Di, Jingen Liu, Jiquan Pei, Jinfeng Yi, and Bowen Zhou. Trustworthy ai: From principles to practices. *ACM Computing Surveys*, 55(9):1–46, 2023. 1

[18] Lin Li, Yifei Wang, Chawin Sitawarin, and Michael Spratling. Oodrobustbench: a benchmark and large-scale analysis of adversarial robustness under distribution shift. *arXiv preprint arXiv:2310.12793*, 2023. 2

[19] Chen Liu, Mathieu Salzmann, Tao Lin, Ryota Tomioka, and Sabine Süsstrunk. On the loss landscape of adversarial training: Identifying challenges and how to overcome them. *Advances in Neural Information Processing Systems*, 33:21476–21487, 2020. 7

[20] Haochen Liu, Yiqi Wang, Wenqi Fan, Xiaorui Liu, Yixin Li, Shaili Jain, Yunhao Liu, Anil Jain, and Jiliang Tang. Trustworthy ai: A computational perspective. *ACM Transactions on Intelligent Systems and Technology*, 14(1):1–59, 2022. 1

[21] Haoyang Liu, Maheep Chaudhary, and Haohan Wang. Towards trustworthy and aligned machine learning: A data-centric survey with causality perspectives. *arXiv preprint arXiv:2307.16851*, 2023. 1, 3

[22] Jianan Ma, Pengfei Yang, Jingyi Wang, Youcheng Sun, Cheng-Chao Huang, and Zhen Wang. Vere: Verification guided synthesis for repairing deep neural networks. In *Proceedings of the 46th IEEE/ACM International Conference on Software Engineering*, pages 1–13, 2024. 1

[23] Divyam Madaan, Jinwoo Shin, and Sung Ju Hwang. Learning to generate noise for multi-attack robustness. In *International Conference on Machine Learning*, pages 7279–7289. PMLR, 2021. 3, 6

[24] Aleksander Madry, Aleksandar Makelov, Ludwig Schmidt, Dimitris Tsipras, and Adrian Vladu. Towards deep learning models resistant to adversarial attacks. *arXiv preprint arXiv:1706.06083*, 2017. 1

[25] Pratyush Maini, Eric Wong, and Zico Kolter. Adversarial robustness against the union of multiple perturbation models. In *International Conference on Machine Learning*, pages 6640–6650. PMLR, 2020. 1

[26] Yuval Netzer, Tao Wang, Adam Coates, Alessandro Bissacco, Baolin Wu, Andrew Y Ng, et al. Reading digits in natural images with unsupervised feature learning. In *NIPS workshop on deep learning and unsupervised feature learning*, page 7. Granada, 2011. 6

[27] Weili Nie, Brandon Guo, Yujia Huang, Chaowei Xiao, Arash Vahdat, and Anima Anandkumar. Diffusion models for adversarial purification. *arXiv preprint arXiv:2205.07460*, 2022. 1

[28] Tianyu Pang, Xiao Yang, Yinpeng Dong, Hang Su, and Jun Zhu. Bag of tricks for adversarial training. *arXiv preprint arXiv:2010.00467*, 2020. 6

[29] Leslie Rice, Eric Wong, and Zico Kolter. Overfitting in adversarially robust deep learning. In *International conference on machine learning*, pages 8093–8104. PMLR, 2020. 6

[30] Herbert Robbins. Some aspects of the sequential design of experiments. 1952. 3

[31] Daniel J Russo, Benjamin Van Roy, Abbas Kazerouni, Ian Osband, Zheng Wen, et al. A tutorial on thompson sampling.

Foundations and Trends® in Machine Learning, 11(1):1–96, 2018. 3

[32] Ali Shafahi, Mahyar Najibi, Mohammad Amin Ghiasi, Zheng Xu, John Dickerson, Christoph Studer, Larry S Davis, Gavin Taylor, and Tom Goldstein. Adversarial training for free! *Advances in neural information processing systems*, 32, 2019. 1, 2

[33] Bing Sun, Jun Sun, Long H Pham, and Jie Shi. Causality-based neural network repair. In *Proceedings of the 44th international conference on software engineering*, pages 338–349, 2022. 1

[34] Christian Szegedy, Wojciech Zaremba, Ilya Sutskever, Joan Bruna, Dumitru Erhan, Ian Goodfellow, and Rob Fergus. Intriguing properties of neural networks. *arXiv preprint arXiv:1312.6199*, 2013. 1, 2

[35] William R Thompson. On the likelihood that one unknown probability exceeds another in view of the evidence of two samples. *Biometrika*, 25(3/4):285–294, 1933. 3

[36] Florian Tramer and Dan Boneh. Adversarial training and robustness for multiple perturbations. *Advances in neural information processing systems*, 32, 2019. 3, 6

[37] Hongjun Wang and Yisen Wang. Self-ensemble adversarial training for improved robustness. *arXiv preprint arXiv:2203.09678*, 2022. 6

[38] Yisen Wang, Yichuan Mo, Hongjun Wang, Junyi Li, and Zhouchen Lin. Generalist++: A meta-learning framework for mitigating trade-off in adversarial training. *arXiv preprint arXiv:2510.13361*, 2025. 2

[39] Zekai Wang, Tianyu Pang, Chao Du, Min Lin, Weiwei Liu, and Shuicheng Yan. Better diffusion models further improve adversarial training. In *International conference on machine learning*, pages 36246–36263. PMLR, 2023. 1

[40] Hui Wei, Hao Tang, Xuemei Jia, Zhixiang Wang, Hanxun Yu, Zhubo Li, Shin’ichi Satoh, Luc Van Gool, and Zheng Wang. Physical adversarial attack meets computer vision: A decade survey. *IEEE Transactions on Pattern Analysis and Machine Intelligence*, 46(12):9797–9817, 2024. 3

[41] Zeming Wei, Yifei Wang, Yiwen Guo, and Yisen Wang. CfA: Class-wise calibrated fair adversarial training. In *Proceedings of the IEEE/CVF conference on computer vision and pattern recognition*, pages 8193–8201, 2023. 1, 6

[42] Eric Wong, Leslie Rice, and J Zico Kolter. Fast is better than free: Revisiting adversarial training. *arXiv preprint arXiv:2001.03994*, 2020. 2

[43] Chaowei Xiao, Jun-Yan Zhu, Bo Li, Warren He, Mingyan Liu, and Dawn Song. Spatially transformed adversarial examples. *arXiv preprint arXiv:1801.02612*, 2018. 1

[44] Cihang Xie, Yuxin Wu, Laurens van der Maaten, Alan L Yuille, and Kaiming He. Feature denoising for improving adversarial robustness. In *Proceedings of the IEEE/CVF conference on computer vision and pattern recognition*, pages 501–509, 2019. 1

[45] Hongyang Zhang, Yaodong Yu, Jiantao Jiao, Eric Xing, Laurent El Ghaoui, and Michael Jordan. Theoretically principled trade-off between robustness and accuracy. In *International conference on machine learning*, pages 7472–7482. PMLR, 2019. 1, 5, 7

[46] Richard Zhang, Phillip Isola, Alexei A Efros, Eli Shechtman, and Oliver Wang. The unreasonable effectiveness of deep features as a perceptual metric. In *Proceedings of the IEEE conference on computer vision and pattern recognition*, pages 586–595, 2018. 3

[47] Yihua Zhang, Guanhua Zhang, Prashant Khanduri, Mingyi Hong, Shiyu Chang, and Sijia Liu. Revisiting and advancing fast adversarial training through the lens of bi-level optimization. In *International Conference on Machine Learning*, pages 26693–26712. PMLR, 2022. 7

A. Theoretical Foundations of MAB Algorithms

This section provides a concise theoretical formulation and comparative analysis of two foundational algorithms for the stochastic multi-armed bandit (MAB) problem: the Upper Confidence Bound (UCB) algorithm and Thompson Sampling.

A.1. Problem Formulation

We consider a stochastic multi-armed bandit with K arms. When an arm $a \in \{1, \dots, K\}$ is pulled at time t , it yields a reward r_t drawn from a fixed but unknown distribution with mean μ_a . The objective of a policy π is to maximize the cumulative reward over a horizon T , or equivalently, to minimize the cumulative pseudo-regret R_T :

$$R_T = T\mu^* - \mathbb{E} \left[\sum_{t=1}^T \mu_{a_t} \right] \quad (12)$$

where $\mu^* = \max_a \mu_a$ is the reward mean of the optimal arm.

A.2. Upper Confidence Bound (UCB) Algorithm

The UCB algorithm is a deterministic method grounded in the optimism in the face of the uncertainty principle. The core idea is to maintain an optimistic estimate of each arm's reward potential and select the arm with the highest upper confidence bound.

Let $\hat{\mu}_a(t)$ be the empirical mean reward of arm a after it has been pulled $n_a(t)$ times by round t . The Chernoff-Hoeffding inequality states that for bounded random variables $X_i \in [0, 1]$:

$$\mathbb{P}(|\hat{\mu}_a - \mu_a| \geq \varepsilon) \leq 2 \exp(-2n_a(t)\varepsilon^2) \quad (13)$$

Applying this to arm a after $n_a(t)$ pulls:

$$\mathbb{P}(|\hat{\mu}_a(t) - \mu_a| \geq \varepsilon) \leq 2 \exp(-2n_a(t)\varepsilon^2) \quad (14)$$

We want to find $U_a(t)$ such that:

$$\mathbb{P}(\mu_a > \hat{\mu}_a(t) + U_a(t)) \leq \delta \quad (15)$$

Setting the right-hand side equal to δ :

$$\exp(-2n_a(t)U_a(t)^2) = \delta \quad (16)$$

Solving for $U_a(t)$:

$$-2n_a(t)U_a(t)^2 = \ln \delta U_a(t)^2 = \frac{-\ln \delta}{2n_a(t)} U_a(t) = \sqrt{\frac{-\ln \delta}{2n_a(t)}} \quad (17)$$

Choosing $\delta = t^{-2}$ to ensure the sum of failure probabilities converges:

$$U_a(t) = \sqrt{\frac{-\ln(t^{-2})}{2n_a(t)}} = \sqrt{\frac{\ln t}{n_a(t)}} \quad (18)$$

The UCB algorithm uses a slightly more conservative bound:

$$\text{UCB}_a(t) = \hat{\mu}_a(t) + \sqrt{\frac{2 \ln t}{n_a(t)}} \quad (19)$$

This ensures that the probability of overestimating any arm's true mean value decreases quickly over time.

This leads to the UCB index for each arm a :

$$\text{UCB}_a(t) = \hat{\mu}_a(t) + \sqrt{\frac{2 \ln t}{n_a(t)}} \quad (20)$$

The algorithm selects the arm a_t at time t as:

$$a_t = \arg \max_a \left[\hat{\mu}_a(t) + \sqrt{\frac{2 \ln t}{n_a(t)}} \right] \quad (21)$$

The first term, $\hat{\mu}_a(t)$, encourages exploitation favoring arms with high empirical rewards. The second term, the confidence bonus, promotes exploration of less frequently pulled arms.

Algorithm 2 UCB Algorithm

- 1: Initialize: Pull each arm once
- 2: **for** $t = K + 1, K + 2, \dots, T$ **do**
- 3: **for** each arm $a = 1, \dots, K$ **do**
- 4: Compute $\text{UCB}_a(t) = \hat{\mu}_a(t) + \sqrt{\frac{2 \ln t}{n_a(t)}}$
- 5: **end for**
- 6: Pull arm $a_t = \arg \max_a \text{UCB}_a(t)$
- 7: Observe reward r_t
- 8: Update $\hat{\mu}_{a_t}(t)$ and $n_{a_t}(t)$
- 9: **end for**

A.3. Thompson Sampling Algorithm

Thompson Sampling is a probabilistic, Bayesian approach to the MAB problem. It maintains a posterior distribution over each arm's mean reward. At every round, a reward estimate is sampled from each posterior, and the arm with the highest sampled value is chosen.

1. **Initialization:** Assume a prior distribution for the mean reward of each arm. For Bernoulli rewards, a natural choice is the Beta distribution, $\text{Beta}(\alpha_a, \beta_a)$, initialized with $\alpha_a = 1, \beta_a = 1$ (a uniform prior).
2. **Loop at each time t :**
 - For each arm a , sample a value $\theta_a(t)$ from its current posterior distribution $\text{Beta}(\alpha_a, \beta_a)$.

- Select the arm $a_t = \arg \max_a \theta_a(t)$.
- Observe the reward $r_t \in \{0, 1\}$.
- Update the posterior distribution for the chosen arm:

$$\alpha_{a_t} \leftarrow \alpha_{a_t} + r_t, \quad \beta_{a_t} \leftarrow \beta_{a_t} + (1 - r_t) \quad (22)$$

Intuitively, the sampling step automatically balances exploration and exploitation. An arm with high uncertainty (a wide posterior) has a higher chance of being sampled with a high value θ_a , even if its current empirical mean is low. As an arm is pulled more often, its posterior distribution narrows around the true mean, and the sampled values become more consistent. For Thompson Sampling, a frequentist regret bound of $O(\ln T)$ has also been established.

Algorithm 3 Thompson Sampling for Bernoulli Bandits

```

1: Initialize:  $\alpha_a = 1, \beta_a = 1$  for all arms  $a = 1, \dots, K$ 
2: for  $t = 1, 2, \dots, T$  do
3:   for each arm  $a = 1, \dots, K$  do
4:     Sample  $\theta_a(t) \sim \text{Beta}(\alpha_a, \beta_a)$ 
5:   end for
6:   Pull arm  $a_t = \arg \max_a \theta_a(t)$ 
7:   Observe reward  $r_t$ 
8:   Update:  $\alpha_{a_t} \leftarrow \alpha_{a_t} + r_t, \beta_{a_t} \leftarrow \beta_{a_t} + (1 - r_t)$ 
9: end for

```

A.4. Regret Analysis

The regret analysis for both algorithms relies on bounding the number of times a suboptimal arm is selected. Let $\Delta_a = \mu^* - \mu_a$ be the suboptimality gap of arm a . For UCB, it can be shown that:

$$\mathbb{E}[n_a(T)] \leq \frac{8 \ln T}{\Delta_a^2} + O(1) \quad (23)$$

which leads to the regret bound:

$$R_T \leq \sum_{a: \Delta_a > 0} \left(\frac{8 \ln T}{\Delta_a} + O(1) \right) \quad (24)$$

For Thompson Sampling, a similar logarithmic regret bound can be established through Bayesian regret analysis or frequentist techniques, though the derivation is more involved due to the probabilistic nature of the algorithm.

A.5. CAS Method Selection

The Thompson Sampling approach assumes that rewards follow a fixed, known distribution (such as normal distribution or Beta distribution). However, in the fine-tuning process with multiple robustness, it is difficult to determine which specific probability distribution the rewards follow. The UCB algorithm avoids this issue and is more convenient in practice. Furthermore, their regret upper bounds

are relatively similar. Therefore, in the CAS method, we have chosen the UCB algorithm to balance exploration and exploitation.

B. Theoretical Details and Proofs

Setup and assumptions. Let $\mathcal{R}_p(\theta)$ and $\mathcal{R}_q(\theta)$ denote robust risks for two attack families $\mathcal{S}_p, \mathcal{S}_q$:

$$\mathcal{R}_i(\theta) = \mathbb{E}_{(x,y) \sim \mathcal{S}_i} \left[\max_{\delta \in \Delta_i} \mathcal{L}(f_\theta(x + \delta), y) \right], \quad i \in \{p, q\}. \quad (25)$$

Define the average robust risk

$$\mathcal{R}_{avg}(\theta) = \frac{1}{2} (\mathcal{R}_p(\theta) + \mathcal{R}_q(\theta)) \quad (26)$$

We make the following local regularity assumptions:

Assumption 1 (Danskin and interchange) For almost every (x, y) the inner maximizer $\delta_i^*(\theta; x, y)$ is locally unique and sufficiently smooth in a neighborhood of θ_1 , so that the pointwise map $\ell_i(\theta; x, y) := \max_{\delta \in \Delta_i} \mathcal{L}(f_\theta(x + \delta), y)$ is differentiable at θ_1 . Furthermore, there exists an integrable dominating function $g(x, y)$ such that $\|\nabla_\theta \ell_i(\theta; x, y)\| \leq g(x, y)$ in a neighborhood of θ_1 . Under these conditions differentiation and expectation may be interchanged, yielding $\nabla \mathcal{R}_i(\theta_1) = \mathbb{E}_{(x,y) \sim \mathcal{S}_i} [\nabla_\theta \ell_i(\theta_1; x, y)]$.

Assumption 2 (Second-order regularity) \mathcal{R}_{avg} is twice continuously differentiable in a neighborhood of θ_1 , with Hessian $H_{avg} := \nabla^2 \mathcal{R}_{avg}(\theta_1)$. Let $\lambda_{\max}(H_{avg})$ denote its largest eigenvalue at θ_1 .

Assumption 3 (Positive spectral direction) We assume that the Hessian matrix H_{avg} of \mathcal{R}_{avg} at θ_1 is not negative semi-definite, i.e., $\lambda_{\max}(H_{avg}) > 0$. Otherwise, \mathcal{R}_{avg} would attain a local maximum at θ_1 . This would imply that, after adversarial training with respect to \mathcal{R}_q , the average robust risk over \mathcal{S}_p and \mathcal{S}_q reaches a local maximum with respect to the model parameters. Such a case is not only mathematically of measure zero but also contradicts the intuition of adversarial training.

Parameter drift formulation. Let the second fine-tuning phase move parameters by $\Delta\theta := \theta_2 - \theta_1$. In the small-step approximation we assume $\Delta\theta$ is aligned with the negative gradient of \mathcal{R}_q , i.e. $\Delta\theta = -\eta \nabla \mathcal{R}_q(\theta_1)$ for small $\eta > 0$. Define the alignment angle ψ between $\nabla \mathcal{R}_{avg}(\theta_1)$ and $\nabla \mathcal{R}_q(\theta_1)$ by

$$\nabla \mathcal{R}_{avg}(\theta_1)^\top \Delta\theta = -\|\nabla \mathcal{R}_{avg}(\theta_1)\| \|\Delta\theta\| \cos \psi. \quad (27)$$

Lemma 1 (Average robust risk bound) The change in average robust risk can be bounded as:

$$\Delta \mathcal{R}_{avg} \lesssim -\|\nabla \mathcal{R}_{avg}(\theta_1)\| \|\Delta\theta\| \cos \psi + \frac{1}{2} \lambda_{\max}(H_{avg}) \|\Delta\theta\|^2 \quad (28)$$

Where ψ denotes the angle between $\nabla\mathcal{R}_{avg}(\theta_1)$ and $\nabla\mathcal{R}_q(\theta_1)$, H_{avg} is the local Hessian of \mathcal{R}_{avg} , $\lambda_{\max}(H_{avg})$ denote its largest eigenvalue at θ_1 .

Proof 1 Expanding \mathcal{R}_{avg} around θ_1 gives

$$\begin{aligned}\mathcal{R}_{avg}(\theta_2) - \mathcal{R}_{avg}(\theta_1) &= \nabla\mathcal{R}_{avg}(\theta_1)^\top \Delta\theta \\ &+ \frac{1}{2} \Delta\theta^\top H_{avg} \Delta\theta + O(\|\Delta\theta\|^3).\end{aligned}\quad (29)$$

Ignoring $O(\|\Delta\theta\|^3)$ for small steps, let

$$\mathcal{R}_{avg}(\theta_2) - \mathcal{R}_{avg}(\theta_1) \approx \nabla\mathcal{R}_{avg}(\theta_1)^\top \Delta\theta + \frac{1}{2} \Delta\theta^\top H_{avg} \Delta\theta \quad (30)$$

Using the spectral upper bound $\Delta\theta^\top H_{avg} \Delta\theta \leq \lambda_{\max}(H_{avg}) \|\Delta\theta\|^2$, we obtain:

$$\Delta\mathcal{R}_{avg} \lesssim -\|\nabla\mathcal{R}_{avg}(\theta_1)\| \|\Delta\theta\| \cos\psi + \frac{1}{2} \lambda_{\max}(H_{avg}) \|\Delta\theta\|^2 \quad (31)$$

This scaling is conservative. If the update direction $\hat{\Delta} = \Delta\theta/\|\Delta\theta\|$ is known, the quadratic term can be tightened to $\frac{1}{2} R(H_{avg}, \hat{\Delta}) \|\Delta\theta\|^2$, where $R(H_{avg}, \hat{\Delta})$ is the Rayleigh quotient about H_{avg} and the direction of $\hat{\Delta}$.

Proposition 1 (Safe parameter-drift threshold) Let $\lambda_{\max}(H_{avg})$ denote the largest eigenvalue of the local Hessian of \mathcal{R}_{avg} at θ_1 . A sufficient condition to prevent average robustness degradation after the sequential fine-tuning in the order of S_p followed by S_q is:

$$\|\Delta\theta\| < \frac{2\|\nabla\mathcal{R}_{avg}(\theta_1)\| \cos\psi}{\lambda_{\max}(H_{avg})}, \quad \psi < \frac{\pi}{2} \quad (32)$$

Proof 2 Based on Lemma 1, a sufficient condition to ensure that the average robust risk continues to decrease under parameter drift is:

$$\begin{aligned}\Delta\mathcal{R}_{avg} &\lesssim -\|\nabla\mathcal{R}_{avg}(\theta_1)\| \|\Delta\theta\| \cos\psi \\ &+ \frac{1}{2} \lambda_{\max}(H_{avg}) \|\Delta\theta\|^2 < 0\end{aligned}\quad (33)$$

Assuming $H_{avg}(\theta_1)$ is not negative semi-definite, so that $\lambda_{\max}(H_{avg}) > 0$, solving the inequality for $\|\Delta\theta\|$ yields the safe threshold:

$$\|\Delta\theta\| < \frac{2\|\nabla\mathcal{R}_{avg}(\theta_1)\| \cos\psi}{\lambda_{\max}(H_{avg})} \quad (34)$$

Hence, if $\|\Delta\theta\|$ exceeds this bound, sequential fine-tuning may increase \mathcal{R}_{avg} , i.e., reduces average robustness. \square

Remarks.

- The bound in Proposition 1 is sufficient but not necessary. It is conservative because of the spectral upper bound used on the Hessian term; a tighter estimate of the Rayleigh quotient yields a less conservative threshold.

- In practice the quantities $\|\nabla\mathcal{R}_{avg}\|$, $\cos\psi$ and $\lambda_{\max}(H_{avg})$ may be estimated from mini-batches and Hessian-vector products (e.g. via power iteration / Pearlmutter products). Because of sampling noise these estimates should be treated as guidance rather than absolute thresholds.

C. Multi-Objective Optimization Perspective on Cross-Type Trade-off

C.1. Externality-Aware Equilibrium

When training proceeds for a sufficiently long period, the uncertainty in reward estimation diminishes as each perturbation type has been sampled enough times. In this asymptotic regime, the influence of the exploration term in the UCB score becomes negligible, since

$$\lim_{t \rightarrow \infty} \sqrt{\frac{2 \log N}{N_v}} \rightarrow 0, \quad (35)$$

and the sampling probability in Eq. (10) simplifies to a softmax-augmented exploitation form:

$$\pi_v \propto w_v \cdot \exp(\alpha \cdot R_v), \quad (36)$$

where $R_v = R_v^{\text{self}} + R_v^{\text{tradeoff}}$ includes both marginal and cross-type effects.

This asymptotic distribution represents an *externality-aware equilibrium*, in which the long-term sampling behavior aligns with the relative overall contribution of each perturbation type to system-wide robustness. Perturbations that yield positive spillover effects naturally gain higher long-run probabilities, while those producing negative externalities are suppressed.

Consequently, the CAS algorithm converges to a stable allocation on the Pareto frontier, where the equilibrium mixture of perturbation types reflects not only their intrinsic robustness importance (w_v) but also their dynamic rewards (R_v). This leads to a self-organizing and globally balanced fine-tuning process.

C.2. Pareto-Frontier Perspective on Cross-Type Trade-off

From a multi-objective optimization perspective, the process of adversarial fine-tuning across multiple perturbation types can be viewed as searching along a Pareto frontier of robustness objectives $\{\mathcal{R}_{p_1}, \dots, \mathcal{R}_{p_M}\}$. Each objective corresponds to robustness under one adversarial type, and jointly optimizing them inevitably involves trade-offs.

In the standard setting, the overall optimization direction is determined by the weighted gradient aggregation

$$\nabla_{\theta} \mathcal{R}_{avg} = \sum_{k=1}^M w_k \nabla_{\theta} \mathcal{R}_{p_k}, \quad (37)$$

where w_k reflects the static relative importance of each perturbation type. This aggregation assumes that improvements in one objective do not introduce externalities to others, which is violated in practice. For instance, improving robustness against ℓ_∞ attacks may slightly degrade robustness against blur or color-shift perturbations, forming a locally concave Pareto surface.

To explicitly account for such cross-type interactions, the CAS method introduces a cross-type trade-off term into the reward formulation. This mechanism dynamically adjusts the effective sampling weights according to each type's net contribution (positive or negative) to the global robustness improvement. Geometrically, this modification changes the optimization trajectory from a fixed-weight combination

$$\sum_k w_k \nabla_\theta \mathcal{R}_{p_k} \quad (38)$$

to a reweighted direction

$$\sum_k w_k \nabla_\theta \mathcal{R}_{p_k} * \exp(\alpha R_k), \quad (39)$$

that effectively steering the update vector toward regions of the Pareto frontier with higher joint gains. Instead of optimizing only along a pre-defined linear scalarization of the objectives, CAS adaptively reshapes the frontier traversal according to dynamic inter-type feedback, allowing the fine-tuning process to converge toward more globally balanced robustness equilibria.

In summary, introducing cross-type trade-off terms transforms the optimization landscape from a static scalarized objective into a *dynamically calibrated Pareto search*. By rewarding perturbation types that produce positive spillover effects and penalizing those inducing interference, CAS achieves more equitable and globally efficient convergence across heterogeneous robustness objectives.

C.3. Economic Motivation Behind Pareto Frontier and Reward Design in CAS

The concept of the Pareto frontier in multi-objective learning is directly inspired by the notion of *Pareto efficiency* in economics, which characterizes an allocation where no objective can be improved without worsening another. In the context of multi-robustness optimization, each perturbation type can be regarded as an “agent” competing for model capacity—a limited resource analogous to economic capital or utility. The CAS framework extends this analogy by introducing *externality-aware rewards*, effectively capturing how the training on one perturbation type influences others.

This heuristic motivation underscores a deep parallel: In the presence of externalities, the free market mechanism cannot automatically achieve Pareto optimality, and government or institutional intervention becomes necessary. According to the Coase theorem, the problem of externalities does not lie in the existence of costs themselves, but

in the failure to assign these costs correctly, that is, to internalize them. We extend this idea to multi-robustness fine-tuning, by internalizing the impact of each adversarial training component on other robustness dimensions within the reward design. From an economic standpoint, the inclusion of cross-type trade-off terms resembles a system of *Pigouvian adjustments*, where positive externalities are rewarded and negative ones are penalized to achieve social welfare optimality. Here, the “social welfare” corresponds to the collective robustness performance across all perturbation types, and CAS dynamically regulates training probabilities to approximate this welfare-optimal equilibrium.

D. Convergence Analysis of CAS Method

In this section, we provide a rigorous convergence analysis for our proposed CAS method under the Robbins-Monro conditions for stochastic approximation.

D.1. Problem Formulation

The CAS method addresses the multi-robust fine-tuning problem through stochastic optimization. Let $\theta \in \mathbb{R}^d$ denote the model parameters and \mathcal{A} represent a finite set of adversarial attack types. We define a probability distribution π over \mathcal{A} that governs the selection of attack types during fine-tuning.

For each attack type $a \in \mathcal{A}$, we have a corresponding loss function $\mathcal{L}_a(\theta, p_a)$, where p_a encapsulates the specific parameters and configuration of attack a . The overall objective of CAS is to minimize the expected risk:

$$\mathcal{L}(\theta) = \mathbb{E}_{a \sim \pi} [\mathcal{L}_a(\theta, p_a)] \quad (40)$$

The CAS optimization procedure employs Stochastic Gradient Descent (SGD) with the following update rule at each iteration t :

$$\theta_{t+1} = \theta_t - \eta_t \nabla_\theta \mathcal{L}_{a_t}(\theta_t, p_{a_t}) \quad (41)$$

where a_t is sampled independently from π at each iteration, and $\nabla_\theta \mathcal{L}_{a_t}(\theta_t, p_{a_t})$ represents the stochastic gradient with respect to parameters θ .

D.2. Theoretical Assumptions

To establish convergence guarantees for CAS, we adopt the following standard assumptions:

Assumption 4 (Learning Rate Schedule) *The sequence of learning rates $\{\eta_t\}_{t=1}^\infty$ satisfies the Robbins-Monro conditions:*

$$\sum_{t=1}^{\infty} \eta_t = \infty \quad \text{and} \quad \sum_{t=1}^{\infty} \eta_t^2 < \infty \quad (42)$$

This ensures adequate exploration while asymptotically eliminating stochastic noise.

Assumption 5 (Smoothness of Loss Function) The expected loss function $\mathcal{L}(\theta)$ is continuously differentiable and μ -strongly convex for some $\mu > 0$. Formally, for all $\theta, \phi \in \mathbb{R}^d$:

$$\mathcal{L}(\phi) \geq \mathcal{L}(\theta) + \nabla \mathcal{L}(\theta)^\top (\phi - \theta) + \frac{\mu}{2} \|\phi - \theta\|^2 \quad (43)$$

Assumption 6 (Unbiased and Bounded Gradients) The stochastic gradients in CAS are unbiased estimators of the true gradient:

$$\mathbb{E}_{a_t \sim \pi} [\nabla_\theta \mathcal{L}_{a_t}(\theta, p_{a_t})] = \nabla_\theta \mathcal{L}(\theta) \quad \text{for all } \theta \quad (44)$$

and exhibit bounded variance:

$$\mathbb{E}_{a_t \sim \pi} [\|\nabla_\theta \mathcal{L}_{a_t}(\theta, p_{a_t}) - \nabla_\theta \mathcal{L}(\theta)\|^2] \leq \sigma^2 \quad \text{for all } \theta \quad (45)$$

This implies bounded second moments: There exists a G such that $\mathbb{E}[\|\nabla_\theta \mathcal{L}_{a_t}(\theta_t, p_{a_t})\|^2] \leq G^2$.

D.3. Main Convergence Theorem

Theorem 1 (Convergence of CAS) Under assumptions above, the sequence of parameters $\{\theta_t\}_{t=1}^\infty$ generated by the CAS update rule:

$$\theta_{t+1} = \theta_t - \eta_t \nabla_\theta \mathcal{L}_{a_t}(\theta_t, p_{a_t}) \quad (46)$$

converges almost surely to the optimal solution θ^*

Proof 3 We prove Theorem 1 using the Robbins-Siegmund almost supermartingale convergence framework.

Let $V_t = \frac{1}{2} \|\theta_t - \theta^*\|^2$ define a Lyapunov function measuring the squared distance to optimum. The CAS update can be expressed as $\theta_{t+1} = \theta_t - \eta_t g_t$, where $g_t = \nabla_\theta \mathcal{L}_{a_t}(\theta_t, p_{a_t})$. Analyzing the evolution of V_t :

$$\begin{aligned} V_{t+1} - V_t &= \frac{1}{2} \|\theta_{t+1} - \theta^*\|^2 - \frac{1}{2} \|\theta_t - \theta^*\|^2 \\ &= \frac{1}{2} \|\theta_t - \eta_t g_t - \theta^*\|^2 - \frac{1}{2} \|\theta_t - \theta^*\|^2 \quad (47) \\ &= -\eta_t g_t^\top (\theta_t - \theta^*) + \frac{\eta_t^2}{2} \|g_t\|^2 \end{aligned}$$

Taking conditional expectation with respect to the filtration \mathcal{F}_t (the history up to iteration t):

$$\begin{aligned} \mathbb{E}[V_{t+1} - V_t \mid \mathcal{F}_t] &= -\eta_t \mathbb{E}[g_t \mid \mathcal{F}_t]^\top (\theta_t - \theta^*) + \frac{\eta_t^2}{2} \mathbb{E}[\|g_t\|^2 \mid \mathcal{F}_t] \quad (48) \\ &= -\eta_t \nabla \mathcal{L}(\theta_t)^\top (\theta_t - \theta^*) + \frac{\eta_t^2}{2} \mathbb{E}[\|g_t\|^2 \mid \mathcal{F}_t] \end{aligned}$$

We now apply our theoretical assumptions. By the smoothness of expected loss function:

$$\nabla \mathcal{L}(\theta_t)^\top (\theta_t - \theta^*) \geq \mathcal{L}(\theta_t) - \mathcal{L}(\theta^*) + \frac{\mu}{2} \|\theta_t - \theta^*\|^2 \geq \mu V_t \quad (49)$$

since $\mathcal{L}(\theta_t) - \mathcal{L}(\theta^*) \geq 0$.

By the unbiased and bounded gradients:

$$\mathbb{E}[\|g_t\|^2 \mid \mathcal{F}_t] \leq G^2 \quad (50)$$

Substituting these bounds:

$$\mathbb{E}[V_{t+1} - V_t \mid \mathcal{F}_t] \leq -\eta_t \mu V_t + \frac{\eta_t^2}{2} G^2 \quad (51)$$

This inequality satisfies the conditions of the Robbins-Siegmund Almost Supermartingale Convergence Theorem. Specifically, since $\sum_{t=1}^\infty \eta_t^2 < \infty$, so:

$$\begin{aligned} \sum_{t=1}^T \eta_t \mu V_t &\leq \sum_{t=1}^T (-\mathbb{E}[V_{t+1} - V_t \mid \mathcal{F}_t] + \frac{\eta_t^2}{2} G^2) \\ &= \frac{G^2}{2} \sum_{t=1}^T \eta_t^2 + \mathbb{E}[V_1 - V_{T+1} \mid \mathcal{F}_t] < \infty \end{aligned} \quad (52)$$

Given that $\sum_{t=1}^\infty \eta_t = \infty$, the convergence of $\sum \eta_t V_t$ necessitates that $V_t \rightarrow 0$ almost surely. The convergence of $\sum_{t=1}^T \eta_t \mu V_t$ also directly implies $\theta_t \rightarrow \theta^*$. This completes the proof of convergence for our CAS method.

D.4. Discussion and Implications

The convergence analysis confirms that CAS provides a principled approach for multi-robust fine-tuning, with guaranteed convergence to an optimal solution that balances robustness across multiple adversarial threat models.

Note that in our proof, we did not use any specific information about the sampling distribution π . Therefore, the proof is equally applicable to both the SAT and E-AT methods. Clearly, the proof also applies to the multi-objective learning method AVG.

E. Empirical Analysis of Trade-off Matrix

The trade-off matrix presented in Figure 6 provides a comprehensive quantitative view of the complex interactions between different adversarial perturbation types during sequential fine-tuning. This analysis reveals critical insights into the Pareto-optimal navigation strategy employed by our CAS method.

E.1. Matrix Structure and Interpretation

The trade-off matrix establishes a systematic framework for understanding how training on one perturbation type influences robustness against others. Each entry represents the directional effect between perturbation pairs, where positive values indicate beneficial transfer, negative values reveal detrimental interference, and near-zero values suggest independence. Diagonal entries are mostly positive, confirming that attack-specific training enhances self-robustness, while

off-diagonal values reveal substantial trade-offs. (The phenomenon that some adversarial training even reduces its own robustness may be due to the loss landscape being unsmoothed at the early stage of fine-tuning, leading to unstable robustness. Increasing the number of fine-tuning epochs for each attack type in sequential fine-tuning might help prevent this issue.) The row and column sums serve as aggregate indicators of each perturbation type’s overall impact on the multi-objective robustness landscape.

E.2. Dominant Positive Transfer Patterns

Analysis reveals that certain perturbation types serve as powerful catalysts for broad robustness improvements. Gabor filter attacks emerge as particularly effective, demonstrating widespread positive transfer across multiple perturbation families including norm-based attacks and elastic transformations. This suggests that Gabor training induces features with generalizable robustness properties. Similarly, L1 attacks show strong self-improvement coupled with positive spillover effects, particularly benefiting geometric and weather-based perturbations. These patterns indicate that carefully selected perturbation types can transcend their specific domains to enhance overall model resilience, providing valuable guidance for efficient multi-objective optimization.

E.3. Problematic Negative Transfer Cases

Conversely, several perturbation types exhibit consistently detrimental effects on overall robustness. JPEG compression demonstrates the most severe negative transfer. Wood perturbations similarly show widespread interference, particularly compromising robustness against common corruptions. These findings highlight the critical importance of identifying and mitigating such negative transfer effects, as indiscriminate training on problematic perturbation types can undermine the entire multi-robustness objective through destructive interference.

E.4. Asymmetric Transfer Relationships

The matrix reveals intriguing asymmetric relationships where transfer effects differ dramatically based on directionality. For instance, while Linf training moderately benefits L2 robustness, the reverse relationship proves detrimental, with L2 training actually degrading Linf performance. Similar asymmetries appear between elastic and snow perturbations, where snow training has disproportionately negative effects on elastic robustness compared to the reciprocal relationship. These directional dependencies underscore the limitations of symmetric treatment in multi-perturbation training and emphasize the need for carefully calibrated, direction-aware sampling strategies.

E.5. Implications for Reward Design

The empirical patterns observed in the trade-off matrix provide strong validation for our cross-type reward design. The systematic quantification of transfer effects enables intelligent navigation toward Pareto-optimal regions where positive transfer dominates, while avoiding conflict zones where robustness objectives severely compete. By dynamically incorporating these relationships into the reward mechanism, our approach naturally favors perturbation types that serve as robustness catalysts while penalizing those causing destructive interference. This data-driven strategy transforms the complex multi-objective optimization problem into a tractable navigation task, where the trade-off matrix serves as both validation of our approach and guidance for its continuous refinement.

F. Ablation Study

The roles of R^{tradeoff} and UCB. As shown in Table 4, removing R^{tradeoff} consistently leads to a noticeable performance drop across all datasets, especially in terms of robustness metrics. This indicates that R^{tradeoff} plays a crucial role in mitigating cross-type trade-offs by explicitly guiding the optimization toward a better Pareto frontier. In contrast, the removal of UCB shows only a slight degradation in robustness, while clean accuracy remains nearly unchanged. This suggests that UCB mainly stabilizes training by adaptively adjusting the sampling of attack types according to their estimated uncertainty, rather than directly contributing large numerical gains. Therefore, R^{tradeoff} primarily governs the effectiveness of robustness trade-off learning, while UCB enhances training stability and ensures consistent convergence across diverse attack distributions.

Epochs. Figure 7 and Figure 8 illustrates the evolution of clean and robust accuracy during fine-tuning on the CIFAR-10 and CIFAR-100 datasets across different adversarial training schemes. For CIFAR-10, robust accuracy rapidly improves within the first 10 epochs, after which performance stabilizes. The clean accuracy fluctuates in the early stage and then converges to a stable level, indicating that moderate fine-tuning epochs are sufficient to achieve a balance between clean and robust performance. In contrast, for CIFAR-100, the overall accuracy levels are lower due to the increased task difficulty. Clean accuracy rises gradually from 45% to around 60%, whereas robust accuracy improves from 15% to about 28% over 20 epochs, showing slower convergence and higher sensitivity to training instability. In particular, the clean accuracy still exhibits unstable fluctuations even after 20 epochs. These results suggest that a longer fine-tuning schedule benefits datasets with higher complexity (e.g., CIFAR-100), where the loss landscape is more irregular and the optimization process requires more iterations to stabilize. Conversely, excessive fine-tuning on

Attacks Trained



Figure 6. Detailed visualization of the trade-off matrix. In the figure, each number represents the change in robust accuracy for its corresponding attack type after the sequential fine-tuning against designated types. Each row shows the data fine-tuned against the adversarial attack labeled on the left; each column shows the data evaluated after being tested with the attack labeled above.

Table 4. Ablation study about the component of R^{tradeoff} and UCB. Both the definitions and the calculation of **avg.** ℓ_p and **avg. Corruption** are the same as in the main experiment. The table reports the average results over five independent runs on three datasets.

Dataset	Method	Clean	avg. Robust	avg. ℓ_p	avg. Semantic
CIFAR-10	CAS	85.26	51.79	52.91	50.67
	CAS w/o R^{tradeoff}	84.40	51.42	52.70	50.14
	CAS w/o UCB	85.08	51.65	52.80	50.51
CIFAR-100	CAS	58.54	27.99	29.23	26.75
	CAS w/o R^{tradeoff}	58.00	27.54	28.77	26.32
	CAS w/o UCB	58.68	27.76	28.50	27.01
Dataset	Method	Clean	avg. Robust	avg. Corruption	avg. Others
SVHN	CAS	93.86	57.76	63.81	51.71
	CAS w/o R^{tradeoff}	94.24	55.77	62.59	48.94
	CAS w/o UCB	93.80	57.59	63.52	51.66

simpler datasets (e.g., CIFAR-10) yields diminishing returns and may even introduce mild overfitting. Overall, Our choice of 10 epochs achieves a good balance between time cost and performance across different datasets.

Hyperparameters. Table 5 presents the ablation results of the hyperparameters α and β , which respectively control the trade-offs between exploration-exploitation and clean-robust performance. When varying α under a fixed $\beta = \frac{8}{9}$, we observe that moderate values (around $\alpha = 5$ –10) consistently yield a good balance between clean and robust accuracy across datasets. Smaller α leads to underexploitation, limiting the improvement of robustness, whereas excessively large α overemphasizes exploitation and harms clean accuracy and robustness due to unstable parameter updates. In contrast, adjusting β while fixing $\alpha = 10$ reveals that increasing β gradually shifts the model’s focus toward robustness, improving average robust accuracy but with sacrifices in clean performance. This trend is more evident on CIFAR-10, where robustness gains saturate beyond $\beta = \frac{8}{9}$, suggesting that too strong a robustness constraint reduces optimization flexibility. However, different dataset tasks exhibit distinct preferences for the hyperparameters. For instance, CIFAR-10 favors larger values of α (around 10–20), while CIFAR-100 and SVHN achieve better performance when α is set between 5 and 10. A value of $\beta = \frac{8}{9}$ provides a good balance between clean accuracy and robustness for CIFAR-10 and CIFAR-100, whereas for SVHN, clean accuracy saturates more easily, and using a larger β can further enhance robustness with relatively minor impact on clean accuracy. Across all datasets, the best configurations emerge when α and β are jointly balanced, supporting our design intuition that moderate exploration and a proportional robustness weighting lead to stable and well-generalized models.

G. Promising Research Directions

Finally, we reflect on the study’s limitations and outline promising research directions:

1. Advancing trade-off characterization: Rigorous benchmarking frameworks or novel theoretical frameworks for multi-robustness trade-offs are waiting to be developed.
2. Expanding attack typology: New adversarial constraints could be proposed, or existing semantic attacks refined through granular categorization to clarify robustness conflicts/synergies.
3. Exploring composite perturbations: Stronger attacks may emerge from strategically combined perturbation types.
4. Formalizing non-algorithmic attacks: Attacks lacking clear algorithmic definitions warrant alternative formalizations or methodological innovations for systematic study.

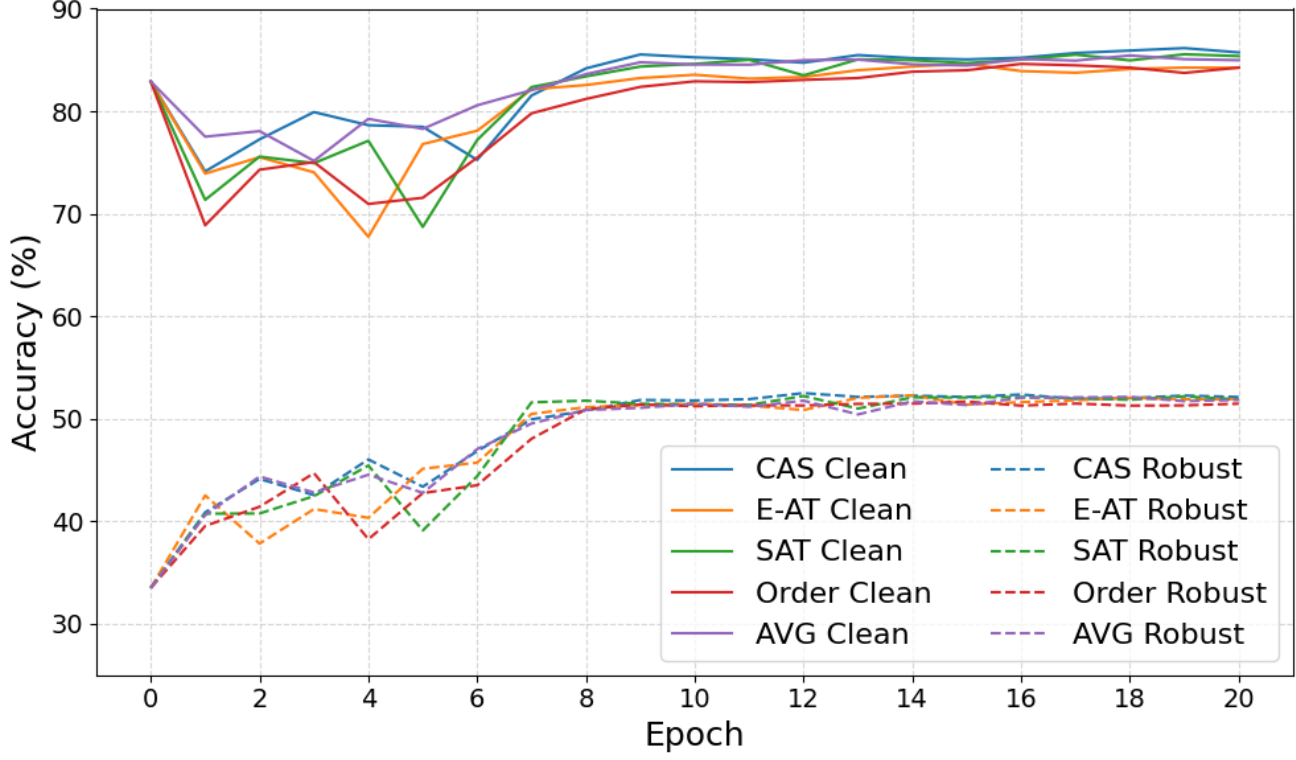


Figure 7. Ablation analysis on training epochs, conducted on the CIFAR-10 dataset. Robust accuracy is the weighted average; all accuracy values are means of five independent runs.

Table 5. Sensitivity analysis on hyperparameters α and β , where α is used to balance exploration and exploitation, and β is used to balance clean accuracy and robustness. The results in the table are averaged over five independent runs.

Dataset	$\beta = \frac{8}{9}, \alpha = ?$	1	5	10	20	50	$\alpha = 10, \beta = ?$	$\frac{1}{2}$	$\frac{2}{3}$	$\frac{4}{5}$	$\frac{8}{9}$	$\frac{16}{17}$
CIFAR-10	Clean	84.32	84.68	85.26	85.42	85.04	Clean	86.02	85.76	85.36	85.26	85.12
	avg. Robust	51.68	51.50	51.79	51.55	50.83	avg. Robust	50.42	50.96	51.45	51.79	51.81
	avg. ℓ_p	53.10	53.27	52.91	52.83	50.60	avg. ℓ_p	51.19	51.99	52.36	52.91	52.90
	avg. Semantic	50.26	49.73	50.67	50.26	51.05	avg. Semantic	49.66	49.93	50.55	50.67	50.73
CIFAR-100	Clean	58.46	58.62	58.54	58.12	57.48	Clean	58.88	58.74	58.50	58.54	58.46
	avg. Robust	27.68	28.05	27.99	27.88	27.61	avg. Robust	27.46	27.77	28.01	27.99	28.08
	avg. ℓ_p	28.89	29.37	29.23	28.87	28.03	avg. ℓ_p	28.74	29.00	29.30	29.23	29.29
	avg. Semantic	26.47	26.72	26.75	26.89	27.19	avg. Semantic	26.28	26.53	26.71	26.75	26.87
SVHN	Clean	93.80	93.98	93.86	93.58	92.98	Clean	94.03	93.87	93.89	93.86	93.82
	avg. Robust	57.45	57.73	57.76	57.62	57.17	avg. Robust	57.41	57.61	57.68	57.76	57.90
	avg. Corruption	63.57	63.81	63.81	63.48	62.36	avg. Corruption	63.35	63.70	63.80	63.81	63.84
	avg. Others	51.32	51.64	51.71	51.77	51.99	avg. Others	51.47	51.53	51.55	51.71	51.96

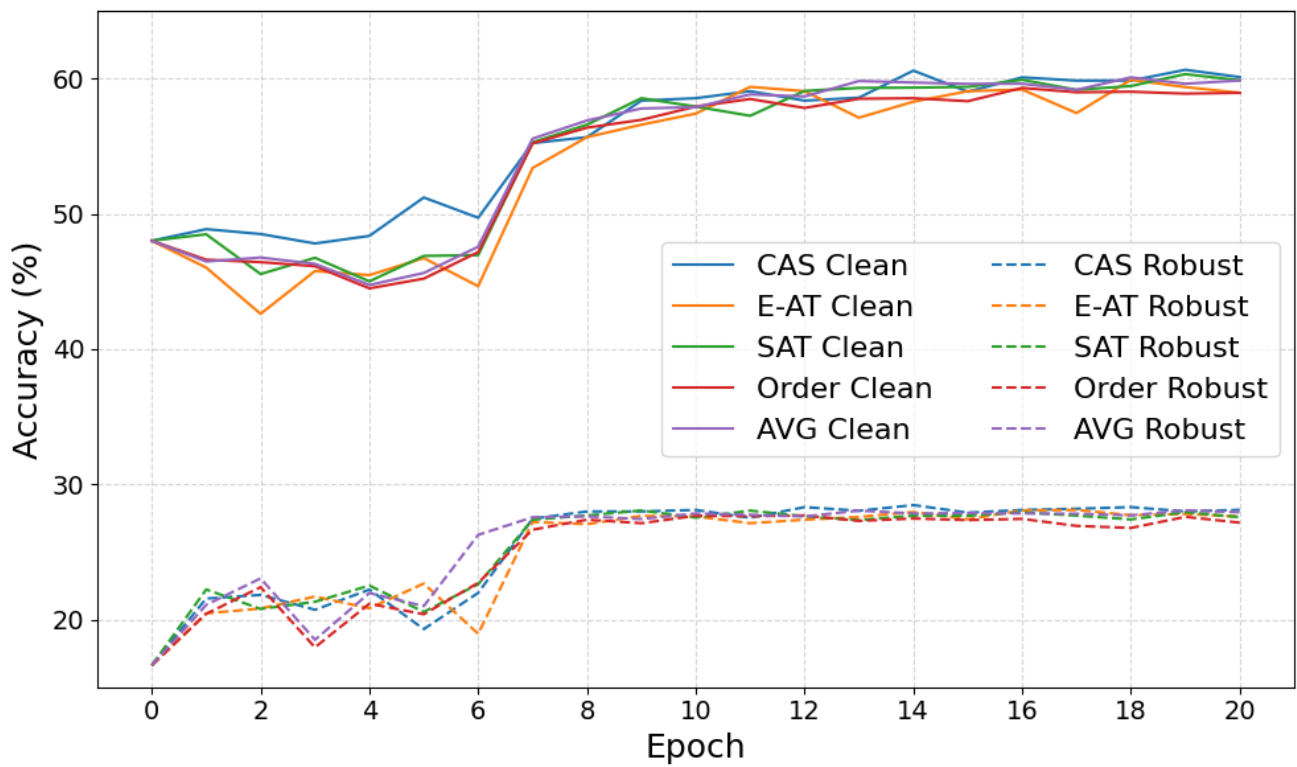


Figure 8. Ablation analysis on training epochs, conducted on the CIFAR-100 dataset. Robust accuracy is the weighted average; all accuracy values are means of five independent runs.